Optical study on the possible Slater insulator $SrIr_{0.8}Sn_{0.2}O_3$

P. Zheng,[1] Q. Cui,[1,2] Z. G. Chen,[1] J. G. Cheng,[1,2,3] X. Liu,[1,4] Z. Q. Wang,[5] and J. L. Luo[1,2,3]

[1]*Beijing National Laboratory for Condensed Matter Physics, Institute of Physics, Chinese Academy of Sciences, Beijing 100190, People's Republic of China*

[2]*School of Physical Sciences, University of Chinese Academy of Sciences, Beijing 100190, China*

[3]*Songshan Lake Materials Laboratory, Dongguan, Guangdong 523808, China*

[4]*School of Physical Science and Technology, ShanghaiTech University, Shanghai 201210, China*

[5]*Department of Physics, Boston College, Chestnut Hill, Massachusetts 02467, USA*

(Received 19 April 2019; revised manuscript received 14 June 2019; published 2 July 2019)

The orthorhombic perovskite iridate $SrIr_{0.8}Sn_{0.2}O_3$ is reported to be a new candidate of Slater insulator at low temperatures. Here, we present optical spectroscopy measurements on $SrIr_{0.8}Sn_{0.2}O_3$ at different temperatures (T) across the paramagnetic-antiferromagnetic phase transition. The low energy reflectivity decreases with reducing T. Six phonon peaks in the spectrum at low T are visible at room temperature, indicating the absence of crystal structure phase transition from 300 K to 10 K. The real part of conductivity spectra $\sigma_1(\omega)$ are obtained by employing the standard Kramers-Kronig transformation. In the paramagnetic state at room temperature, $\sigma_1(\omega)$ reaches a limiting value as $\omega \to 0$, implying an electrical conducting state. Upon decreasing T, the low frequency $\sigma_1(\omega)$ decreases and approaches zero with a concomitant opening of a direct gap. Detailed analysis of the low energy data shows that the gap opening is continuous and $\sigma_1(\omega)$ at the low energy gap edge follows an unusual $\omega^{1/2}$ dependence at low temperatures which is remarkably similar to other Slater insulators, such as $NaOsO_3$.

DOI: 10.1103/PhysRevB.100.045101

I. INTRODUCTION

The metal-insulator (MI) transition is one of the most important phenomena in the condensed matter physics and has attracted much attention over half a century. Various mechanisms have been proposed to drive a paramagnetic conducting system into an insulating phase, such as the Mott MI transition [1] and Slater MI transition [2], etc. In the Mott MI transition, the Coulomb blocking due to the on-site electron-electron correlation (EEC) causes the opening of the Mott gap and the localization of the electrons. There are no coherent bandlike excitations [1,3,4]. An antiferromagnetic (AF) order usually develops by the exchange coupling of the local moments in the Mott insulator. The Slater MI transition, on the other hand, is expected from an itinerant picture in an AF environment. In the Slater transition, an electron of spin up has lower potential energy in the atoms with net spin up than in those with net spin down. Consequently there is a periodic alternation of potential from the atoms with one net spin to those with the other. Taking into account the perturbation of the Hartree-Fock potential, the energy difference will split the band into two: a lower and a higher subband separated by a band gap [2]. For a half-filled band, the lower subband will be completely filled and the higher band empty, i.e., the AF order alone could produce an insulating state by doubling the unit cell [2]. Consequently, the Slater MI transition is continuous and of second order without crystal structure transition, but with a segregation of itinerant electrons of opposite spins. An important difference between a Slater AF insulator and a Mott AF insulator is there are quasiparticle band excitations in the former, while in the latter case there are no coherent quasiparticle excitations [5].

The Slater model was applied to explain the insulating state in certain one-dimensional situations in the original work [2]. Although the lack of two-dimensional Slater insulator has been discussed in theoretical calculations [6], the possibility of Slater MI transition in three-dimensional compounds has been proposed in Os based oxides [7–11]. The underlying mechanism remains however controversial due to the extreme rareness of the samples. Furthermore, due to the essentially identical order parameter, the two models are difficult to distinguish clearly amid the interplay of EEC, crystal field, and spin-orbital coupling (SOC) effect, and we await more in-depth experimental studies.

The 5*d* transition-metal oxides have emerged as an important system for studying the MI transition. The Sr_2IrO_4 is an AF insulator and a candidate correlated electron material for 5*d* transition-metal oxides [4]. Certain Os based oxides might undergo the Slater MI transition [7–11]. The orthorhombic perovskite $SrIrO_3$ with the space group *Pbnm* is a paramagnetic metal, possibly a doped Dirac semimetal [12], which is believed to sit very close to the MI transition. An enhancement of the thermoelectric power showing a peak at about 175 K could be attributed to the SOC effect [13]. Recently, in the Sn-substituted samples $SrIr_{1-x}Sn_xO_3$, a paramagnetic to AF transition is observed in the temperature dependence of the susceptibility, which is accompanied by a simultaneous change of the electrical transport property in the resistivity curve [13]. For $SrIr_{0.8}Sn_{0.2}O_3$, the critical temperature T_N of paramagnetic to AF insulating phase transition is about 275 K, below which a Bragg peak centered at $Q = 1.377(5)$Å is observed by neutron powder diffraction [13]. Further analysis shows that the peak represents *G*-type AF ordering in the *Pbnm* structure, i.e., a reduced structural

symmetry in the magnetically ordered phase. Based on these observations $SrIr_{1-x}Sn_xO_3$ was referred to as a new Slater insulator [13]. Since the EECs are also important in this system, further studies are needed to characterize this possible Slater insulator.

Optical spectroscopy is a powerful tool to probe the bulk electronic structure and dynamics near the Fermi level. In this paper, we report low-energy optical absorption studies of $SrIr_{0.8}Sn_{0.2}O_3$, covering the whole temperature range from a poor conducting state above the AF transition to an insulating state at low temperatures. The material shows the sharpest phase transition peak in the specific heat curve, implying the purest phase states [13]. The measured real part of the conductivity spectra in the infrared region shows that the optical conductivity decreases significantly but does not vanish when $\omega \to 0$ at 250 K, a temperature slightly smaller than critical temperature T_N. Further analysis reveals that the sample is in the conducting state at room temperature and the MI transition is continuous. In the AF insulating state, we find that the onset of the real part of the conductivity has the power-law behavior $(\omega - E_g)^\alpha$ near the low-energy edge, which is indicative of quasiparticle interband excitations across the insulating gap induced by the AF long-range order. Our findings support that $SrIr_{0.8}Sn_{0.2}O_3$ possess a Slater AF insulating ground state driven by itinerant spin-orbital magnetism in a 3D $5d$ transition metal oxide.

II. EXPERIMENT

Because single crystals of $SrIr_{0.8}Sn_{0.2}O_3$ are not available, we performed the optical study on high density polycrystalline samples prepared under 6 GPa and 1000 °C as described in Ref. [13]. The optical reflectance $R(w)$ was measured from 50 cm^{-1} to 25000 cm^{-1} at different temperatures on a Fourier transform spectrometer (Bruker 80v). The frequency-dependent optical conductivity $\sigma(\omega)$ was derived employing the standard Kramers-Kronig transformation. We use Hagen-Rubens relation at high temperatures and/or constant at low temperatures for the low frequency extrapolations of the reflectance data. We found that the different low-frequency extrapolations do not affect the conductivity spectra in the measured frequency region. On the high frequency side, the measured reflectance curve is extrapolated constantly to 80000 cm^{-1}, above which a well-known function of ω^{-4} is used.

III. RESULTS AND DISCUSSIONS

The reflectivity spectra at various temperatures are plotted in the top panel of Fig. 1. There are many phonon peaks in the low frequency region of the spectra (the bottom one in Fig. 1). All phonons in the low temperature spectra are still visible in the room temperature spectrum. The low frequency reflectivity decreases with sample cooling. Excluding the phonon contributions, all $R(\omega)$ monotonously decreases with increasing frequency. The curves cross near 2000 cm^{-1} and then merge together above 6000 cm^{-1}. Figure 2 is a collection of the real part of the optical conductivity $\sigma_1(\omega)$, which decreases at the low frequency as the sample is cooled from

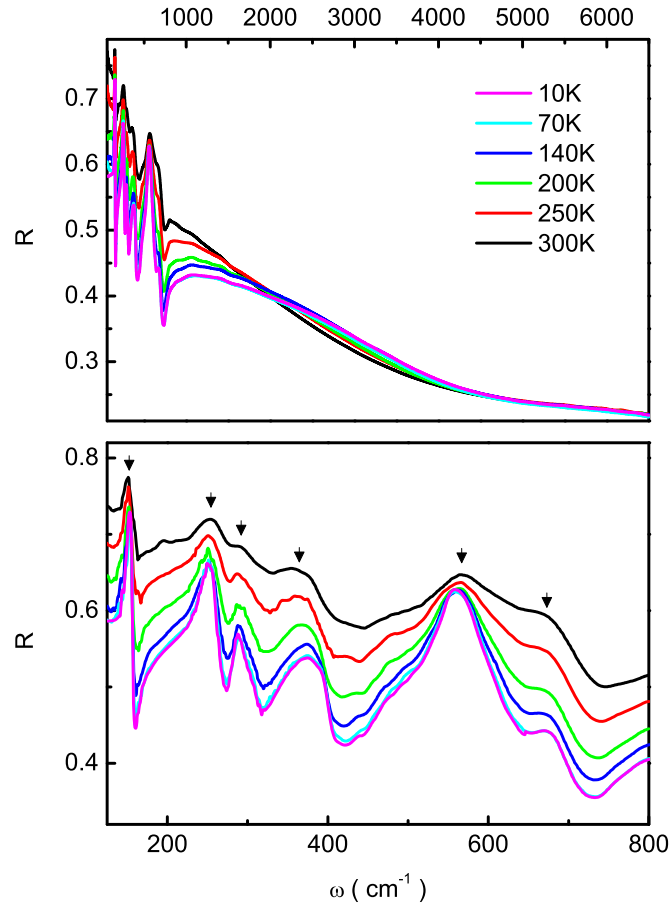

FIG. 1. Top figure is a plot of the frequency dependence of reflectivity $R(w)$ at 300 K, 250 K, 200 K, 140 K, 70 K, and 10 K, respectively. The bottom one displays the phonons in the far-infrared region at different temperatures in an enlarged scaling.

300 K to 10 K, consistent with the temperature dependence of the dc resistivity [13].

The conductivity spectra display a T-independent interband transition peak at about 8000 cm^{-1} (~1 eV) in Fig. 2. According to band calculations of $SrIrO_3$ [12,14,15], the $5d$ bands should be split into twelve low energy t_{2g} bands and eight high energy e_g bands by the IrO_6 octahedral crystal field. The twelve t_{2g} bands further split into low-lying fully occupied $J_{eff} = 3/2$ and high-lying half-filled $J_{eff} = 1/2$ states by the strong SOC. The calculation shows that the splitting between the $J_{eff} = 1/2$ and $J_{eff} = 3/2$ bands increases with the SOC increasing. Considering the higher SOC energy in $SrIr_{0.8}Sn_{0.2}O_3$ than that in $SrIrO_3$ [13], this 8000 cm^{-1} peak could be attributed to the contribution of the interband transition from occupied $J_{eff} = 3/2$ bands to unoccupied $J_{eff} = 1/2$ ones or occupied $J_{eff} = 1/2$ bands to unoccupied e_g bands, which hybridize with O $2p$ bands [12,14].

Now we focus on the low frequency region in the spectra of the real part of the conductivity. In the low-energy spectrum at room temperature, the real part of the optical conductivity in $SrIr_{0.8}Sn_{0.2}O_3$ is *nonzero*. In addition to the phonon features, $\sigma_1(\omega)$ slowly increases with ω in the far-infrared region and reaches a maximum between 800 cm^{-1} and 4000 cm^{-1}. Here a sum of interband transition contribution and a broad Drude

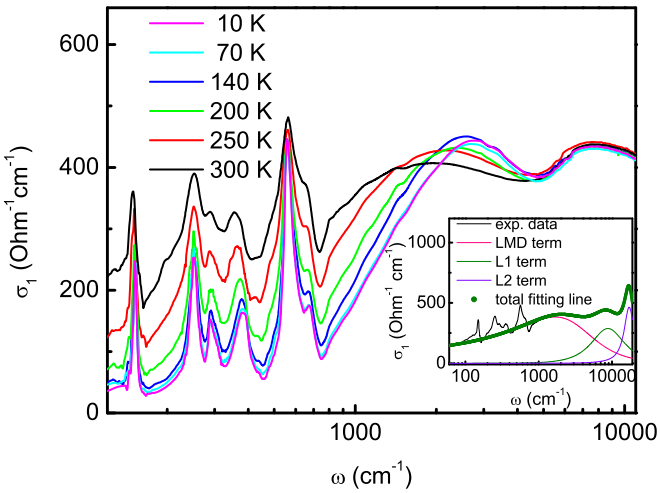

FIG. 2. Real part of optical conductivity $\sigma_1(w)$ at 300 K, 250 K, 200 K, 140 K, 70 K, and 10 K, respectively. The inset: fitting the frequency dependence of σ_1 at 300 K. The solid black line represents the raw data and the green circles are the fitting result using the localization modified Drude-Lorentz model.

contribution could possibly fit the low-energy spectrum. On the other hand, this behavior can be and is usually considered as resulting from the localization of the electron wave function for the conducting carriers. Such a behavior has also been observed in other poor conductors such as $Ca_2Os_2O_7$ [11] and polymer conductors [16]. In those conductors, localization modified Drude model (LMD) in the framework of the Anderson Mott localization theory is widely used to fit the real part of optical conductivity:

$$\sigma_{LMD}(\omega) = \frac{\omega_p^2}{4\pi}\frac{\tau}{(1+\omega^2\tau^2)}\left[1 - \frac{C}{(k_F\upsilon_F)^2\tau^2} + \frac{C}{(k_F\upsilon_F)^2\tau^{3/2}}(3\omega)^{1/2}\right], \quad (1)$$

where ω_p is the plasma frequency and k_F and υ_F are the Fermi wave vector and Fermi velocity with τ the relaxation time. C is a material independent constant of order unity. In view of the not very low resistivity of 10^{-2} $\mathrm{Ohm^{-1}cm^{-1}}$ which is in the bad metal region and for simplicity, we use the LMD model alone to fit the low-energy data. The inset of Fig. 2 shows that the sum of the LMD and two Lorentz peaks could fit the 300 K spectrum well below 20 000 $\mathrm{cm^{-1}}$ with $\omega_p \simeq 8800$ $\mathrm{cm^{-1}}$ and $\tau \simeq 1.04 \times 10^{-14}$ s. The lifetime is about one order of magnitude smaller than that of metals ($\tau > 10^{-13}$ s), suggesting a localization modified itinerant behavior of the charge carriers at room temperature, i.e., a poor metallic state. The value of the parameter $k_F\ell$, where $\ell = \tau\upsilon_F$ is the mean free path, can be estimated using $\tau k_F \upsilon_F/\mathrm{C}$. For the 300 K data, we found that $k_F\lambda$ is about 1.1, which is greater than 1 and puts the material on the metallic side of the metal-insulator transition in terms of Ioffe-Regel criterion $k_F\ell \sim 1$.

The lack of an insulating charge gap in the optical conductivity at temperatures $T > T_N$ and the presence of the itinerate carriers are consistent with the prerequisite of the Slater MI model. Thus the AF insulating state at $T < T_N$ should be considered as a Slater insulator. This is in contrast to the $n = 1$ limit of the Ruddlesden-Popper series $Sr_{n+1}Ir_nO_{3n+1}$, the layered Sr_2IrO_4 which shows high and activated resistivity in the paramagnetic phase above T_N [17], suggesting an AF Mott insulating ground state [18]. It is instructive to consider a simplified picture where the series is viewed as effective Mott-Hubbard systems for the spin-orbit coupled quasiparticles occupying a narrow $J_{eff} = 1/2$ band around the Fermi level. The EEC is represented by the Hubbard U and the bandwidth W. Increasing U/W, we expect an AF order at U_{AF} accompanied by the doubling of the unit cell and a Mott transition at U_{Mott} characterized by the opening of a charge gap [5]. Thus we expect that $U > U_{Mott}, U_{AF}$ in Sr_2IrO_4, such that melting the AF order reveals the Mott insulator with a charge gap above T_N. On the other hand, for the 3D $SrIrO_3$, the paramagnetic metallic ground state suggests $U < U_{Mott}, U_{AF}$, i.e., the metallic side of both the Mott and the AF transition. Fractional substitution of Ir^{4+} by Sn^{4+} causes a narrowing of the $J_{eff} = 1/2$ band and thus an increase in the effective interaction strength U/W [13]. It is thus conceivable that our findings put $SrIr_{0.8}Sn_{0.2}O_3$ in the regime $U_{AF} < U < U_{Mott}$, realizing a Slater AF insulator with a poor metallic state above T_N. Within this picture, increasing the EEC (U/W) further can in principle realize the Mott transition inside the AF ordered state proposed theoretically [5].

Next, we turn to the properties of the low-temperature AF insulating state. When the temperature is reduced across the critical point T_N to below 250 K, the low frequency $\sigma_1(\omega)$ gradually (Fig. 2) decreases and is almost zero below 140 K, suggesting a continuous metal-insulating transition and a gap opening. In the crossover region at 250 K, the gap is small. Upon decreasing temperature further, the gap becomes larger due to the gradual development and then completion of the magnetic phase transition. Meanwhile, the spectral weight contributed by the interband transition crossing the new gap gradually dominates the spectra. The peak centering above 2000 $\mathrm{cm^{-1}}$ comes from the contribution of the interband transition crossing the new opened gap and its maximum shows a continuous blueshift (Fig. 2) until 70 K. In the insulating state, the conductivity below the gap can be best described with a linear dependence

$$\sigma_1(\omega) = m\omega + q \quad \text{for } \omega < E_g \quad (2)$$

and the spectrum near the onset of the low-energy gap edge follows:

$$\sigma_1(\omega) = A(\omega - E_g)^\alpha \quad \text{for } \omega > E_g. \quad (3)$$

The intragap conductivity is due to the contribution from thermally excited carriers across the insulating gap. The function (3) is typical of the direct interband transition in a semiconductor with a band gap E_g [19]. Our best fitting yields $\alpha \simeq 1/2$ as shown in the upper panel of Fig. 3. Note that such a frequency dependence at the low-energy gap edge is different from that of the $5d$ AF Mott insulator Sr_2IrO_4 [4]. It is however expected for a Slater antiferromagnet [2,20] because of the coherent quasiparticle interband excitations and has indeed been confirmed in $NaOsO_3$ [19], where an $E^{-1/2}$ divergence in the density of state $N(E)$ has been argued to produce a real part of conductivity σ_1 that grows with $E^{1/2}$ above the band gap.

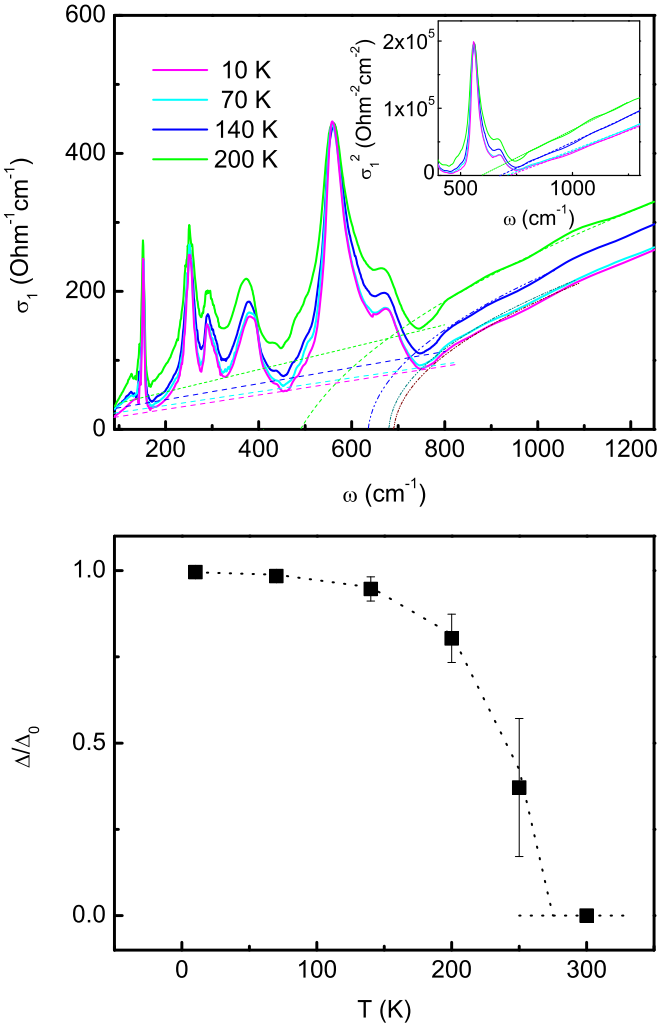

FIG. 3. Upper panel: the low energy region of the $\sigma_1(w)$ spectra at $T < T_{MIT}$. The inset shows the data plotted as the square of the conductivity to display the square root dependence more clearly. The dashed line of $\sigma_1(\omega) \propto (\omega - E_g)^{1/2}$ for each temperature is the expected theoretical frequency dependence of the gap edge in the Slater model. Below the gap edge, a linear fit is used for each data. The crossing of the two fitting lines could be taken as the measurement of the direct gap energy. The measurement results are shown in the lower panel.

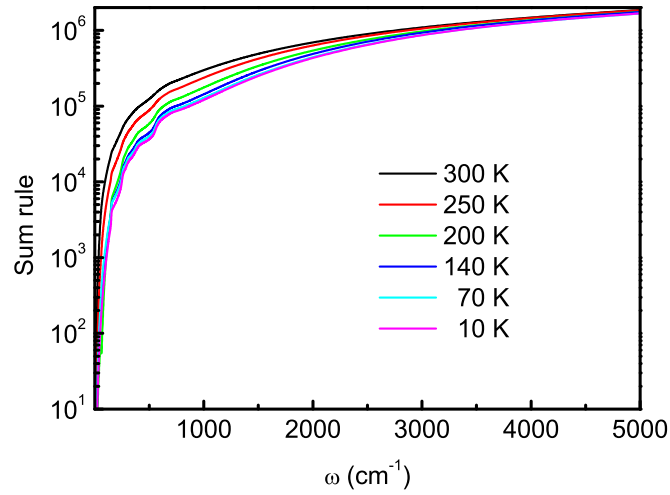

FIG. 4. Effective spectral weight vs cutoff frequency for temperatures from 300 K to 10 K.

The $(\omega - E_g)^{1/2}$ behavior is also recognizable at higher temperatures, although it becomes difficult near and above 250 K. We define the direct gap energy 2Δ by the crossing point of the linear-ω dependent line and the $\omega^{1/2}$ function. The temperature dependence of the normalized energy gap is plotted in the lower panel of Fig. 3, which shows clearly that 2Δ opens at T_N and tends to saturate at low temperatures to $2\Delta_0 \simeq 700$ cm^{-1} ($\sim$0.087 eV). The lower panel of Fig. 3 shows the continuous evolution of the extracted insulating gap 2Δ with decreasing temperature. Remarkably, the gap opens at a metal-insulator transition temperature $T_{MIT} \sim 275$ K, which coincides with the AF transition temperature T_N. Moreover, the gap-to-temperature ratio $2\Delta_0/k_BT_N \approx 3.18$, close to the BCS value for superconductivity in the weak-coupling limit. These findings provide further support that the AF transition is of the Slater type.

The continuous opening of the spectral gap can also be revealed by the variation of the effective spectral weight $N_{eff}(\omega) = 120/\pi \int_0^{\omega} \sigma_1(\omega')d\omega'$ since it is well known that $N_{eff}(\omega)$ is proportional to the number of carriers participating in the optical absorption up to the cutoff frequency ω. For a Slater MI transition, the continuous opening of the gap will reduce the density of conducting carriers. Therefore, a gradually loss of spectra weight in the low energy region is expected as T is decreased from room temperature to 10 K across the AF transition temperature T_N. The obtained $N_{eff}(\omega)$ are plotted in Fig. 4 at different temperatures. A large reduction of N_{eff} is observed in the intragap region and compensated at higher energy with decreasing temperature, while N_{eff} spectra merge together above 4000 cm^{-1}. The reduction in the integrated spectral weight $N_{eff}(\omega)$ at low-energy reveals the conducting carriers are gapped out by the continuous opening of the insulating gap. The carriers in a wide energy range of the order 10Δ are involved in the MI transition. The continuous decreasing of the low frequency $\sigma_1(\omega)$ and the continuous variation of the effective spectral weight are inconsistent with those associated with the Mott MI transition which is generally believed to be discontinuous.

To shed light on whether the above variation of the spectral weight is related to a crystal structure transition, we checked the phonon response in the spectra. In the far-infrared region, the six phonon peaks at 148.8 cm^{-1}, 250.6 cm^{-1}, 290.3 cm^{-1}, 357.0 cm^{-1}, 563.9 cm^{-1}, and 655.0 cm^{-1} in the 300 K optical conductivity spectrum in Fig. 2, which are zoomed in Fig. 5, can also be seen at all lower temperatures. No phonon disappearance or any new phonon peaks emerging could be distinguished upon crossing the MI transition, implying the absence of abrupt crystal structure phase transitions with the sample cooled down to 10 K in both $R(\omega)$ and $\sigma_1(\omega)$. The absence of structural transition is also consistent with the continuous nature of the Slater MI transition. The phonon peaks become more pronounced with decreasing T, but the position is almost temperature independent except for the

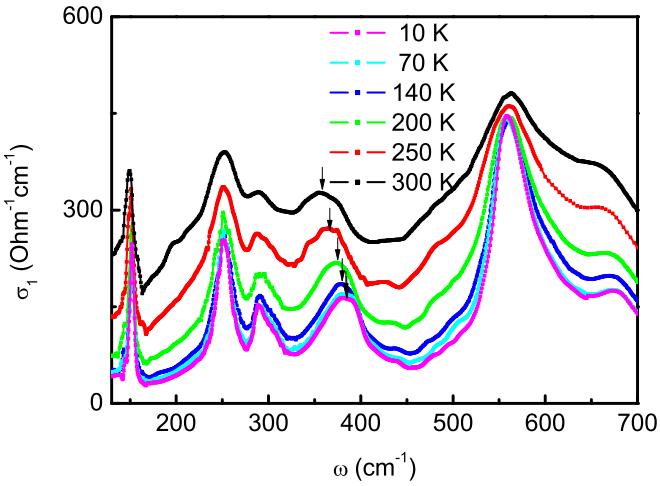

FIG. 5. Phonons in the real part of optical conductivity spectra at 300 K, 250 K, 200 K, 140 K, 70 K, and 10 K in the far infrared frequency region, respectively. The black arrow shows the moving of 357 cm^{-1} with T varying.

357.0 cm^{-1} mode, which gradually moves to 385.0 cm^{-1} as T decreases to 10 K as marked by the arrows in Fig. 5, indicating the corresponding bond shrinking in the crystal structure [21]. As discussed in Ref. [13], $SrIr_{0.8}Sn_{0.2}O_3$ has an orthorhombic perovskite structure with the space group *Pbnm*. Similar to the other orthorhombic perovskite structures [22], the 357 cm^{-1} phonon mode could be assigned to the O-Ir-O deformation vibrations. Our observed blueshift of the 357 cm^{-1} phonon peak should correspond to a continuous shrinking of O-Ir-O bond and not to a crystal structure transition. Usually for the Slater model, a second-order MI transition without crystal structure transition, a collinear-antiferromagnetic ground state, and a distinct $\omega^{1/2}$ of the real part of the conductivity at the gap edge are simultaneously expected [2,19,20]. Our comprehensive optical results thus support the conclusion that MI transition in $SrIr_{0.8}Sn_{0.2}O_3$ is of a Slater type.

IV. SUMMARY

In conclusion, we reported optical reflectance investigations of $SrIr_{0.8}Sn_{0.2}O_3$. Our results revealed that the sample evolves from a poor conductor to an insulator as T decreases across the AF transition, below which an energy gap is observed to develop in the optical measurements. Along with the gap opening, the spectral weight in the low frequency region is transferred to the higher frequency region. The continuous opening of the gap without any phonon emerging and/or annihilated together with an $\omega^{1/2}$ dependence of the conductivity in the low energy gap edge are consistent with a Slater type MI transition.

Note added. Recently, we became aware of an independent optical study on the charge dynamics of $SrIr_{1-x}Sn_xO_3$ [23].

ACKNOWLEDGMENTS

This work is supported by the National Science Foundation of China (Grants No. 11574358, No. 11674375 and No. 11874400), the National Key Research and Development of China (Grants No. 2018YFA0305702, No. 2017YFA0302901 and No. 2016YFA0300303), and U.S. Department of Energy, Basic Energy Sciences, Grant No. DE-FG02-99ER45747 (Z.Q.W.). Chinese Academy of Sciences under Grant No. 112111KYSB20170059.

[1] N. F. Mott, Proc. Phys. Soc. London, Sect. A **62**, 416 (1949); *Metal-Insulator Transitions* (Taylor and Francis, London, Philadelphia, 1990).
[2] J. C. Slater, Phys. Rev. **82**, 538 (1951).
[3] P. A. Cox, R. G. Egdellt, J. B. Goodenough, A. Hamnett, and C. C. Naishj, J. Phys. C **16**, 6221 (1983).
[4] B. J. Kim, H. Jin, S. J. Moon, J.-Y. Kim, B.-G. Park, C. S. Leem, J. Yu, T. W. Noh, C. Kim, S.-J. Oh, J.-H. Park, V. Durairaj, G. Cao, and E. Rotenberg, Phys. Rev. Lett. **101**, 076402 (2008); B. J. Kim, H. Ohsumi, T. Komesu, S. Sakai, T. Morita, H. Takagi, and T. Arima, Science **323**, 1329 (2009).
[5] S. Zhou, Y. P. Wang, and Z. Q. Wang, Phys. Rev. B **89**, 195119 (2014).
[6] S. Moukouri and M. Jarrell, Phys. Rev. Lett. **87**, 167010 (2001).
[7] D. Mandrus, J. R. Thompson, R. Gaal, L. Forro, J. C. Bryan, B. C. Chakoumakos, L. M. Woods, B. C. Sales, R. S. Fishman, and V. Keppens, Phys. Rev. B **63**, 195104 (2001).
[8] W. J. Padilla, D. Mandrus, and D. N. Basov, Phys. Rev. B **66**, 035120 (2002).
[9] J. Yamaura, K. Ohgushi, H. Ohsumi, T. Hasegawa, I. Yamauchi, K. Sugimoto, S. Takeshita, A. Tokuda, M. Takata, M. Udagawa, M. Takigawa, H. Harima, T. Arima, and Z. Hiroi, Phys. Rev. Lett. **108**, 247205 (2012).
[10] S. Calder, V. O. Garlea, D. F. McMorrow, M. D. Lumsden, M. B. Stone, J. C. Lang, J.-W. Kim, J. A. Schlueter, Y. G. Shi, K. Yamaura, Y. S. Sun, Y. Tsujimoto, and A. D. Christianson, Phys. Rev. Lett. **108**, 257209 (2012).
[11] P. Zheng, Y. G. Shi, Q. S. Wu, G. Xu, T. Dong, Z. G. Chen, R. H. Yuan, B. Cheng, K. Yamaura, J. L. Luo, and N. L. Wang, Phys. Rev. B **86**, 195108 (2012).
[12] J. M. Carter, V. V. Shankar, M. A. Zeb, and H.-Y. Kee, Phys. Rev. B **85**, 115105 (2012).
[13] Q. Cui, J.-G. Cheng, W. Fan, A. E. Taylor, S. Calder, M. A. McGuire, J.-Q. Yan, D. Meyers, X. Li, Y. Q. Cai, Y. Y. Jiao, Y. Choi, D. Haskel, H. Gotou, Y. Uwatoko, J. Chakhalian, A. D. Christianson, S. Yunoki, J. B. Goodenough, and J.-S. Zhou, Phys. Rev. Lett. **117**, 176603 (2016).
[14] M. A. Zeb and H.-Y. Kee, Phys. Rev. B **86**, 085149 (2012).
[15] S. J. Moon, J. Korean Phys. Soc. **64**, 1174 (2015).
[16] G. Li, P. Zheng, N. L. Wang, Y. Z. Long, Z. J. Chen, J. C. Li, and M. X. Wan, J. Phys.: Condens. Matter **16**, 6195 (2004).
[17] G. Cao, J. Bolivar, S. McCall, J. E. Crow, and R. P. Guertin, Phys. Rev. B **57**, R11039 (1998).
[18] I. N. Bhatti, R. Rawat, A. Banerjee, and A. K. Pramanik, J. Phys.: Condens. Matter **27**, 016005 (2014).

[19] I. Lo Vecchio, A. Perucchi, P. Di Pietro, O. Limaj, U. Schade, Y. Sun, M. Arai, K. Yamaura, and S. Lupi, Sci. Rep. **3**, 2990 (2013).

[20] G. A. Thomas, D. H. Rapkine, S. A. Carter, A. J. Millis, T. F. Rosenbaum, P. Metcalf, and J. M. Honig, Phys. Rev. Lett. **73**, 1529 (1994).

[21] J. Reading, C. S. Knee, and M. T. Weller, J. Mater. Chem. **12**, 2376 (2002).

[22] C. Shivakumara, Solid State Commun. **139**, 165 (2006).

[23] J. Fujioka, T. Okawa, M. Masuko, A. Yamamoto, and Y. Tokura, J. Phys. Soc. Jpn. **87**, 123706 (2018).